Connectivity Analysis for mmWave V2V Networks: Exploring Critical Distance and Beam Misalignment

Mumin Ozpolat, Osama Alluhaibi, Erik Kampert, and Matthew D. Higgins
WMG, University of Warwick, UK
Email: {M.Ozpolat, O.Alluhaibi, E.Kampert, M.Higgins}@warwick.ac.uk

***Abstract*—In this paper, we investigate the analytical connectivity performance of Vehicle-to-Vehicle communications when using millimeter wave carrier frequencies, by taking into account its challenges of high path loss and beam misalignment. The connectivity analysis is carried out in two dimensions; first, an analytical and parametric critical transmission range is developed, based on system parameters such as vehicle density and Signal-to-Interference-Plus-Noise ratio threshold, and second, the beam misalignment probability caused by the in-lane lateral displacement of vehicles is determined. The analysis is carried out for antennas with half power beamwidths of 3°, 6°, 10°, 20° and 45°, resulting in different beamwidth regimes depending upon road curvature and vehicle density. For low/medium vehicle density on low-curvature roads, the sensitivity of the network connectivity to the beamwidth is relatively small. On the other hand, the narrowest beamwidth is the best performer in terms of maximizing connectivity in low/medium vehicle density scenarios on high-curvature roads, and the wider beamwidth is the best performer for high vehicle density on low-curvature roads.**

I. Introduction

COOPERATIVE driving in the context of connected and autonomous vehicles (CAVs) is a leading automotive research theme within both academia and industry due to its significant and timely potential to enhance and improve safety, traffic flow, fuel consumption and emissions [1]. Fundamentally, cooperative driving is built on the capability to exchange inertia, LiDAR, radar and video, sensor data amongst the vehicles through a wireless channel, with typical implementations as platooning and cooperative adaptive cruise control (CACC) [2]. Thus a situational, real-time, beyond line of sight awareness is enabled without equipping the vehicles with high-cost, long-range sensors or installing frequent road-side units.

The key metric for the reliability of cooperative driving is *connectivity*, the number of connected/disconnected links between a set of vehicles. In Vehicle-to-Vehicle (V2V) communications, disconnected links can occur frequently due to the high-speed mobility of the nodes, thus rapidly changing the network topology and the dynamic node population [3]. The body of literature has investigated V2V connectivity in the frame of 802.11.p and other sub-6 GHz protocols [4] and builds on distance-shortcomings, i.e. the distance between successive vehicles being longer than the critical transmission range, which is the maximum distance that can enable a reliable link between a transceiver pair.

The exchange of giga-byte quantities of data created by LiDAR and cameras is an overwhelming requirement for the aforementioned protocols. Therefore, one of the primary solutions to provide higher data rates, is to use millimeter wave (mmWave) carrier frequencies and directional antenna beams [5] [6]. In addition to distance-based disconnectivity, the use of directional beams will introduce beam misalignment disconnectivity due to the vehicles' mobility.

Disconnectivity of sparse vehicular ad hoc networks based on empirical data was studied in [7] and the critical transmission range for connectivity was studied in [8]. In [9], the mean cluster size and probability of forming single clusters for vehicular ad hoc networks was investigated. However, mmWave communications has not been considered in these works as the focus was on developing an analytical model for a system based on sub-6 GHz communication systems. Hence, [10] considered mmWave communications and used the obstacle size and route relay window relationships to obtain the best connectivity between hops. In vehicular mmWave communications, [11] studied the performance of dual-hop vehicle-to-vehicle (V2V) communications and the best cooperative vehicular relay selection, however, this work was not specifically designed for vehicular connectivity.

Connectivity through mmWave V2V communications has several trade-offs. For example, an increase in vehicle density results in shorter distances for multi-hop communications and thereby improves connectivity, but at the same time it increases the overall interference and deteriorates connectivity performance. In addition, wider beamwidths imply less beam misalignment and thereby improves connectivity, but at the same time it reduces the antenna gain and results in a weaker signal strength, which worsens connectivity. On the other hand, decreasing the beamwidth makes misalignment more likely and thereby worsens the connectivity, but at the same time it increases the antenna gain which causes more powerful signal reception, which results in better connectivity.

To reveal the effective factors on connectivity of mmWave V2V networks, the contributions of this paper can be summarized as

- We present an analytical model, validated by Monte Carlo simulations, which shows the reaction of connectivity performance according to a change of vehicle density, beamwidth, Signal-to-Interference-plus-Noise Ratio (SINR) threshold and antenna gain.
- We introduce a two-dimensional connectivity probability that includes a variable critical transmission range based on SINR-threshold and beam misalignment probability caused by the in-lane lateral displacement of vehicles.

- We introduce beamwidth optimization strategies which show that; (i) the narrowest beam is not the best performer for high-density traffic and low-curvature roads, (ii) connectivity performance has a minor dependence on beamwidth for low and medium vehicle density on low-curvature roads, (iii) significant changes in connectivity performance typically occur only for beams narrower than 10°.

II. System Model

In this paper, a unidirectional, single-lane, vehicular traffic flow is taken into account between two adjacent road side units (RSUs) which are located at the road intersections. The separation distance, D, between two RSUs is illustrated in Fig. 1. The primary purpose of this set-up is the enabling of cooperative driving through the passing of LiDAR and other sensor data between each vehicle in the network and the RSUs through the implementation of multi-hop data transmission. It is assumed that each vehicle is equipped with two mmWave transceiver antennas with corresponding directional-beamforming-providing capabilities. One of the antennas is assumed to be the transmitter and the other a receiver at any moment. It is assumed that each vehicle communicates with the closest vehicle in the same lane either at its front or rear. Furthermore, each vehicle behaves both as a transmitter and a receiver at any moment, as illustrated in Fig. 1.

The close-in path loss model [12], $Ad^{-\alpha}$, is implemented in this work where A is the path loss intercept, parametrized as $(4\pi d_0 f_c/c)^{-2}$ where f_c is the carrier frequency, c is the speed of light, d is the distance between the transmitter-receiver antennas of vehicles, d_0 is the reference distance set as $1\,\mathrm{m}$ and α is the measurement-defined path loss exponential. The path loss exponential is found to be approximately 2 in the most recent measurements [12]. Moreover, the carrier frequency is set to $28\,\mathrm{GHz}$. In addition, the Doppler shift caused by the mobility of vehicles is ignored as directional beams decrease the Doppler shift, and the use of an automated frequency control (AFC) loop at the receiver vehicle could neutralize small Doppler shifts [13].

Empirical VANET (Vehicular Ad Hoc Networks) studies have shown that the number of vehicles that passes an observer point follows a Poisson distribution [14] [7]. We consider a road segment defined by $\mathcal{D} = [0\ D]$ where a vehicle enters the network at position $x = 0$ and leaves at $x = D$. Using the arrival rate of the vehicles, λ_v, the density of the spatial distribution of vehicles on the road is given as

$$\lambda = \lambda_v \int_0^{\infty} \frac{1}{v} d_{f_V} = \lambda_v E(V^{-1}), \tag{1}$$

where f_V is the distribution function of vehicular velocity, V. Thus, the average number of vehicles between two RSUs is $E[N(t)] = \lambda D$ for any time t [3]. By using order statistics and conditional distributions [15], it is revealed that the positions of the vehicles on the road segment $[0\ D]$ form as a Poisson Point Process (PPP).

The curvature of the road, beamwidth and density of vehicles strongly affects the probability of vehicles to interfere with each other. Fig. 1 shows the distribution of interferers for the same road curvature and beamwidth, with a lower number of interfered vehicles in Fig. 1a compared to Fig. 1b, due to fact that the former has a lower vehicle density. Intuitively, vehicles traveling on a straight road will interfere with each other as they will likely stay in the beam propagation region. Also, it is clear that an increased beamwidth will cause higher interference to other vehicles as could be visualized from Fig. 1. Hence, a σ parameter is introduced in order to model the aforementioned issues, which is inversely proportional to the probability of being interfered with.

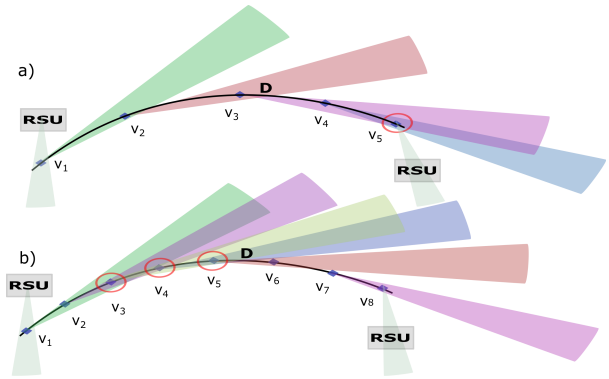

Fig. 1. Graphical representation of vehicles distributed on a curvy road. The intended receiver for the transmitter vehicle, v_i, is v_{i+1}. In (a), note that v_5, the vehicle in the red circle, is an interfered node as it also located in the propagation region of the beam of v_3. In (b), 3 vehicles are interfered nodes.

In the analytical model, the main lobe antenna gain, G_m, and side lobe antenna gain, $0 \leq g_s \ll 1$, are chosen to represent directional beamforming [16], [17]. The main lobe antenna gain is given as

$$G_{i,j} = \begin{cases} G_m = \frac{2\pi - (2\pi - \phi_{i,j})g_s}{\phi_{i,j}}, & \text{if } |\theta_{i,j}(\sigma)| \leq \phi_{i,j}/2, \\ g_s, & \text{otherwise,} \end{cases} \tag{2}$$

where $\phi_{i,j}$ and $\theta_{i,j}(\sigma)$ are the half-power beamwidth and beam alignment error in angular degree between a consecutive transmitter, i, and receiver, j, respectively.

Since the interference of the main and side lobes are different, it is a necessary to thin the density of transmitter/interferers. $\mathbb{P}_{GG}$, $\mathbb{P}_{Gg}$ and $\mathbb{P}_{gg}$ are the probability of main-to-main, main-to-side and side-to-side lobe interference, respectively. In addition, the aforementioned probabilities are dependent on whether the interfering beams propagate towards the receiver's main beam side or its other side. For instance, $\mathbb{P}_{GG}$ can only be formed by the vehicles that are located in the receiver vehicle's beam, i.e. at the front or rear, as both the interferer and receiver beams have to align. The thinning probability of side-to-side lobe interference from the receiver beam side is modeled as $1-\mathbb{P}_{GG}$ whereas the thinning probability of side-to-side lobe interference from the other side is modeled as 0.5. This is due to the fact that half of the interferers are located at the other side and have a 0.5 probability to direct their beams towards the receiver. Moreover, it is assumed that $\mathbb{P}_{Gg}$ can only be formed by the vehicles that are located on the other side. Thus, $\mathbb{P}_{GG}$ is modeled as a two-peak truncated Gaussian random variable

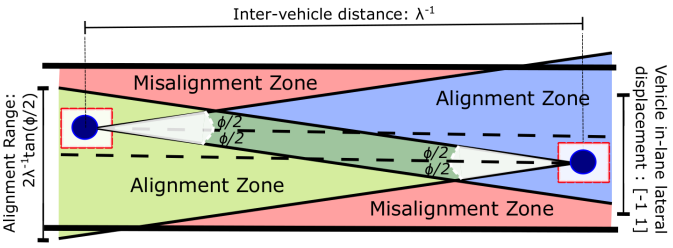

Fig. 2. Characterization of alignment and misalignment regions.

as in [17],

$$\mathbb{P}_{GG}(\sigma) = \frac{1}{2}\int_{-\frac{\phi_{i,j}}{2}}^{\frac{\phi_{i,j}}{2}} \frac{\frac{1}{\sqrt{2\pi}} e^{\frac{-x^2}{2\sigma^2}}}{\frac{\sigma}{2}\left(\text{erf}\left(\frac{\pi/2}{\sqrt{2}\sigma}\right) - \text{erf}\left(\frac{-\pi/2}{\sqrt{2}\sigma}\right)\right)}, \quad (3)$$

where erf is error function and other combinations are given as $\mathbb{P}_{Gg} = 0.5$, $\mathbb{P}_{gg} = 1 - \mathbb{P}_{GG}(\sigma) + 0.5$.

A. Distance-based Connectivity

The connectivity analysis in this work is built on two fundamental branches, namely distance and beam alignment. To be able to connect two adjacent vehicles over a mmWave channel, the receiver vehicle must be located in the critical transmission range of the transmitter vehicle. For the distance-based connectivity analysis, we model the critical transmission range of the transmitter vehicles, r_c, based on a pre-set SINR. In other words, if the receiver SINR is greater than some pre-set threshold, T, then the maximum distance between the adjacent transmitter and receiver pairs that provides a robust and reliable link for SINR $\geq T$ is set as the critical transmission range. The expected value of SINR is given as

$$\mathbb{E}\left(\frac{P_t G_m G_m A r_c^{-\alpha}}{I_\Psi + N_0}\right) \geq T, \quad (4)$$

where P_t, A, α, N_0 are transmitter power, path loss intercept, path loss exponential and zero-mean Gaussian noise magnitude, respectively. Also, I_Ψ is the sum of all interferences and defined as $\sum_{i\epsilon\Psi/\{z\}} P_t G_{i,j} G_{i,j} A r_i^{-\alpha}$ excluding the corresponding transmitter that is located at z. Note that small scale fading is ignored for the purpose of analytical simplification. Also, the blockage effect of obstructing vehicles is omitted due to the fact that the transmitter and receiver antennas are placed on the roof of the vehicles. By extracting the transmitter power, antenna gain and path loss from the expected value in (4), the following is obtained,

$$P_t G_m G_m A r_c^{-\alpha} \mathbb{E}\left(\frac{1}{I_\Psi + N_0}\right) \geq T. \quad (5)$$

After rearranging (5) by converting the inequality to equality, the critical transmission range is defined as

$$r_c = \left(\frac{P_t G_m G_m A \mathbb{E}(\frac{1}{I_\Psi + N_0})}{T}\right)^{1/\alpha}. \quad (6)$$

In order to calculate the expected value in (6), by means of moving the expected value into an integral, it is rewritten as

$$\mathbb{E}\left(\frac{1}{\sum_{i\epsilon\Psi} I_i + N_0}\right) = \int_0^\infty \mathbb{E}\left(e^{-s\left(\sum_{i\epsilon\Psi} I_i\right)}\right) e^{-sN_0} d_s. \quad (7)$$

Thereafter, applying the probability generating functional (PGFL) results in

$$\mathbb{E}\left(\frac{1}{\sum_{i\epsilon\Psi} I_i + N_0}\right) = \int_0^\infty e^{-sN_0} e^{\lambda \mathbb{P}_{GG} \int_R \left(e^{-sP_t G_m^2 A r^{-\alpha}} - 1\right) d_r}$$

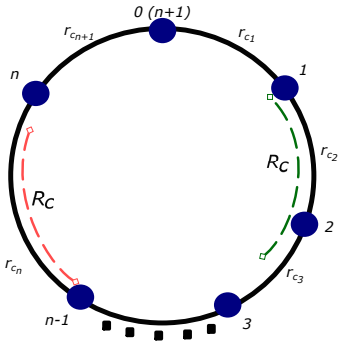

Fig. 3. Graphical representation of the circular distribution of vehicular distances. The red arc, R_c, represents the case in which the critical transmission range is shorter than the required distance to satisfy the SINR threshold. On the other hand, the green arc, R_c, represents the case in which the required distance is shorter than the critical transmission range.

$$\times e^{\lambda \mathbb{P}_{Gg} \int_R \left(e^{-sP_t G_m g_s A r^{-\alpha}} - 1\right) d_r + \lambda \mathbb{P}_{gg} \int_R \left(e^{-sP_t g_s^2 A r^{-\alpha}} - 1\right) d_r} d_s. \quad (8)$$

Finally, the expected value of the inverse of interference and noise is rewritten and presented as

$$\mathbb{E}\left(\frac{1}{\sum_{i\epsilon\Psi} I_i + N_0}\right) = \int_0^\infty e^{-sN_0} \prod_{i\epsilon\psi} F_i d_s, \quad (9)$$

where the ψ set corresponds to $\{GG, Gg, gg\}$ for antenna gains and $\{\mathbb{P}_{GG}, \mathbb{P}_{Gg}, \mathbb{P}_{gg}\}$ for their probabilities in

$$F_i = e^{\lambda \mathbb{P}_i \left(r_f \left(\frac{E_{1+\frac{1}{\alpha}}\left(\frac{sP_t G_i A}{r_f^\alpha}\right)}{\alpha} - 1\right) - r_n \left(\frac{E_{1+\frac{1}{\alpha}}\left(\frac{sP_t G_i A}{r_n^\alpha}\right)}{\alpha} - 1\right)\right)}$$

where $E_{1+\frac{1}{\alpha}}$ is the exponential integral and r_f is chosen as a high number, such as $10D$, in order to take into account the interference of vehicles outside the connectivity region, $\mathcal{D}$, whereas r_n is chosen as $1\,\text{m}$. Insertion of (9) into (6) finalizes the critical transmission range.

B. Misalignment-based Connectivity

The beam misalignment of the transceiver pair can only be caused by in-lane instantaneous lateral displacement of the vehicles. It is assumed that the average lane-width is 3.65m and the average car width is 1.7m. Since the transceiver antennas are placed at the center-top of the vehicles, the lateral displacement range of the antennas is modeled as $\left[-\left(\frac{3.65-1.7}{2}\right) \quad \left(\frac{3.65-1.7}{2}\right)\right]$, which approximately corresponds to $[-1 \quad 1]$. Lateral displacement measurements of [18] have a similar range as shown in Fig. 2. In addition, [19] has measured the lateral distribution of vehicles on UK highways, formed 23 bins. and modeled the probability distribution as Gaussian with mean $\mu = 0$ and standard deviation $\gamma = 0.32$. In this set-up, the probability of the vehicle's center to be located at the position of -1 or 1 is 0.009. Since PPP is applied, the average distance between two consecutive vehicles is λ^{-1}. Thus, half of the width of the transmitter beam's alignment zone at the receiver's location is $\lambda^{-1}\tan\left(\frac{\phi}{2}\right)$ due to the fact that the alignment zone of the beam widens with distance, as is shown in Fig. 2. Therefore, the probability of the receiver antenna to be located in the

alignment zone of the transmitter beam is given as,

$$Q=\int_{-1}^{1}\frac{e^{\frac{-y_t^2}{2\gamma^2}}}{\sqrt{2\pi\gamma^2}}\left(\int_{y_t-\lambda^{-1}\tan\left(\frac{\phi}{2}\right)}^{y_t+\lambda^{-1}\tan\left(\frac{\phi}{2}\right)}\frac{e^{\frac{-y_r^2}{2\gamma^2}}}{\sqrt{2\pi\gamma^2}}dy_r\right)dy_t. \quad (10)$$

where y_t and y_r are the locations of the transmitter and receiver, respectively and (10) can be simplified as

$$Q=\frac{1}{2}\int_{-1}^{1}\frac{e^{\frac{-y_t^2}{2\gamma^2}}}{\sqrt{2\pi\gamma^2}}\left(\operatorname{erf}\left(\frac{y_t+\lambda^{-1}\tan\left(\frac{\phi}{2}\right)}{\gamma\sqrt{2}}\right)-\operatorname{erf}\left(\frac{y_t+\lambda^{-1}\tan\left(\frac{\phi}{2}\right)}{\gamma\sqrt{2}}\right)\right)dy_t. \quad (11)$$

It is geometrically straightforward to prove that if the receiver is located in the alignment region of the transmitter, then the transmitter is located in the alignment region of the receiver.

III. Connectivity Analysis

The probability of entirely covering a unit circle with finite arcs of equal length, where the arcs are uniformly and independently distributed, has been studied thoroughly in the literature [20] [21], also providing the distribution of the gaps, i.e. any point that is not covered by arcs. Interestingly, the resulting mathematical models can be used as a base for V2V connectivity, in which the clockwise initial points of any arc can be modeled as the locations of the transmitter vehicles, and the length of the arcs can be modeled as the critical transmission ranges. Moreover, the occurrence of any gaps can be modeled as disconnected links. By adding misalignment probabilities to the analytical model in order to make it suitable for mmWave V2V networks, a two-dimensional connectivity model is obtained. The arc-based analytical conversion is carried out as follows. First, the distance between two consecutive vehicles at any moment t as shown in Fig. 1 is normalized by D and redistributed on a circle as shown in Fig. 3. Then, the consecutive inter-vehicle distance scaled by D for each vehicle, thus $n+1$ links, is given as,

$$r_{c_i}(t)\triangleq\frac{r_{v_i}(t)}{D},\ i=1,2,...,n+1. \quad (12)$$

Similarly, the scaled SINR-based critical transmission range, R_c, is obtained by using r_c/D. The probability of the ith arc in Fig. 3 to be longer than the scaled critical transmission range, which causes disconnectivity regardless of the connection state of other links, is represented as

$$\mathbb{P}_{\ltimes}(i)\triangleq\mathbb{P}\left(r_{c_i}(t)>R_c, i=1,2,...,n+1|N(t)=n\right). \quad (13)$$

Since disconnectivity can occur due to failure to reach the critical transmission range and due to beam misalignment, it is necessary to examine them individually. The probability that the ith link is solely disconnected by failure to reach the critical transmission distance is given as [20]

$$\mathbb{P}_d(i)=\left(1-iR_c\right)^n \text{ for } i\leq\lfloor R_c^{-1}\rfloor. \quad (14)$$

The probability of misalignment-based disconnectivity between two consecutive vehicles in a network of n vehicles is given as

$$\mathbb{P}_m(i)=(1-Q)^i Q^{n+1-i}. \quad (15)$$

By combining (14) and (15), the probability of the ith link to be disconnected is given as,

$$\mathbb{P}_{\ltimes}(i)=\begin{cases}\sum_{j=0}^{i}\binom{i}{j}(1-Q)^j Q^{i-j}(1-(i-j)R_c)^n, & \text{if } i-j\leq\lfloor R_c^{-1}\rfloor\\ 0, & \text{if } i-j>\lfloor R_c^{-1}\rfloor\end{cases}. \quad (16)$$

The probability of exactly i disconnected links in the whole network is modeled [21] as

$$\widehat{\mathbb{P}}_{\ltimes}(i)=\binom{n+1}{i}\sum_{j=0}^{n+1-i}\binom{n+1-i}{j}(-1)^j\mathbb{P}_{\ltimes}(i+j). \quad (17)$$

Finally, by changing the upper limit of the sum operators [3], the probability of i disconnected links caused by failure to reach the critical transmission range and/or caused by misalignment is summarized as

$$\widehat{\mathbb{P}}_{\ltimes}(i)=\begin{cases}\binom{n+1}{i}\sum_{j=0}^{\lfloor R_c^{-1}\rfloor-i}\binom{n+1-i}{j}(-1)^j\mathbb{P}_{\ltimes}(i+j), & \text{if } i\leq\lfloor R_c^{-1}\rfloor\\ 0, & \text{if } i>\lfloor R_c^{-1}\rfloor\end{cases}. \quad (18)$$

IV. Analysis and Discussion

In this section, we analytically analyze the connectivity performance, validated by Monte Carlo simulations with more than 10^6 iterations, by means of counting the number of disconnected links in a network by changing parameters such as vehicle density, frequency of in-lane communications/interference, SINR threshold and beamwidth. The effect of beamwidth is investigated for 5 different values, $3^\circ, 6^\circ, 10^\circ, 20^\circ, 45^\circ$ in order to sample from narrow to wide beamwidth. The parameters of the analysis are set as follows: $g_s=0.1$, $P_t=1\,\mathrm{W}$ and $N_0=-86.86\,\mathrm{dBm}$ for $500\,\mathrm{MHz}$. The vehicle density per lane is gradually increased from Fig. 4 to Fig. 5 and Fig. 6. Accordingly, the number of links are calculated by using $\lambda D+1$, which includes both RSU links. Zero disconnected links means that the vehicular network is end-to-end connected.

The σ, which is implemented in (3) in order to control the main-to-main lobe interference probability, $\mathbb{P}_{GG}$, is used accordingly to shape the probability of main-to-side and side-to-side lobe interferences. A lower σ implies that a vehicle's beam is more likely to propagate in the same lane, which results in more interference to vehicles in the lane. On the other hand, a higher σ implies that the vehicle's beam is more likely to propagate out of the lane, which results in less interference for those vehicles. In order to analyze two cases, σ is set as 1 or 5, which simulates low- and high-curvature roads, respectively. In the $\sigma=1$ case, the main-to-main lobe interference probabilities of $3^\circ, 6^\circ, 10^\circ, 20^\circ, 45^\circ$ beamwidth scenarios, $\mathbb{P}_{GG}(\sigma)$, are 0.43, 0.49, 0.5, 0.5 and 0.5, whereas in the $\sigma=5$ case they are 0.12, 0.23, 0.34, 0.47, 0.5, respectively. Because of the assumption that beams propagate towards the vehicles only from the front or the rear, the maximum probability of main-to-main lobe interference is set as 0.5. Also, since the road curvature and vehicle density have a stronger effect for narrow beamwidths, a higher

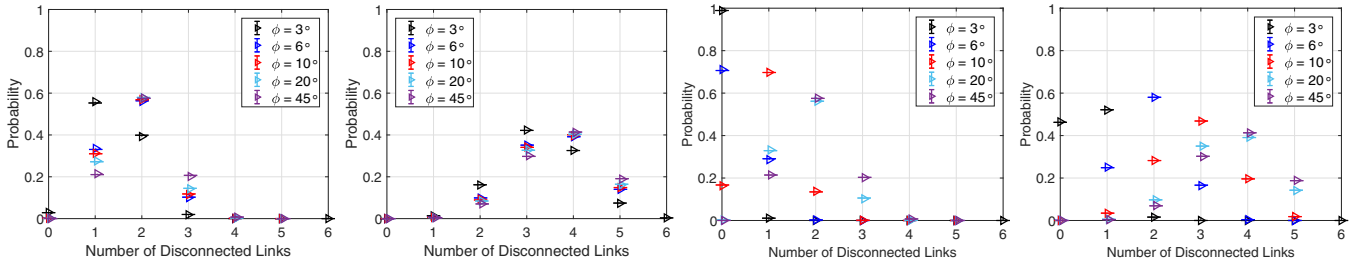

(a) $\lambda = 0.005$, $\sigma = 1$, $T = 3\,\mathrm{dB}$ (b) $\lambda = 0.005$, $\sigma = 1$, $T = 10\,\mathrm{dB}$ (c) $\lambda = 0.005$, $\sigma = 5$, $T = 3\,\mathrm{dB}$ (d) $\lambda = 0.005$, $\sigma = 5$, $T = 10\,\mathrm{dB}$

Fig. 4. Low vehicle density case with triangle markers and horizontal lines displaying the analytical and simulation results, respectively. Average inter-vehicle distance is $200\,\mathrm{m}$ and $D = 1000\,\mathrm{m}$.

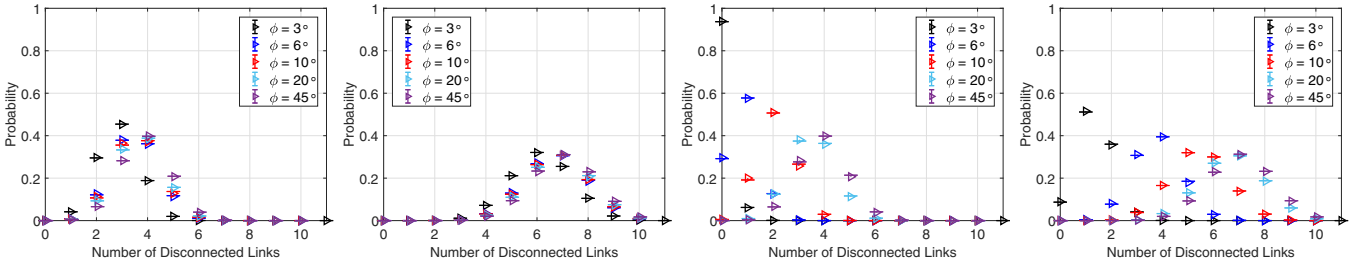

(a) $\lambda = 0.01$, $\sigma = 1$, $T = 3\,\mathrm{dB}$ (b) $\lambda = 0.01$, $\sigma = 1$, $T = 10\,\mathrm{dB}$ (c) $\lambda = 0.01$, $\sigma = 5$, $T = 3\,\mathrm{dB}$ (d) $\lambda = 0.01$, $\sigma = 5$, $T = 10\,\mathrm{dB}$

Fig. 5. Medium vehicle density case with triangle markers and horizontal lines displaying the analytical and simulation results, respectively. Average inter-vehicle distance is $100\,\mathrm{m}$ and $D = 1000\,\mathrm{m}$.

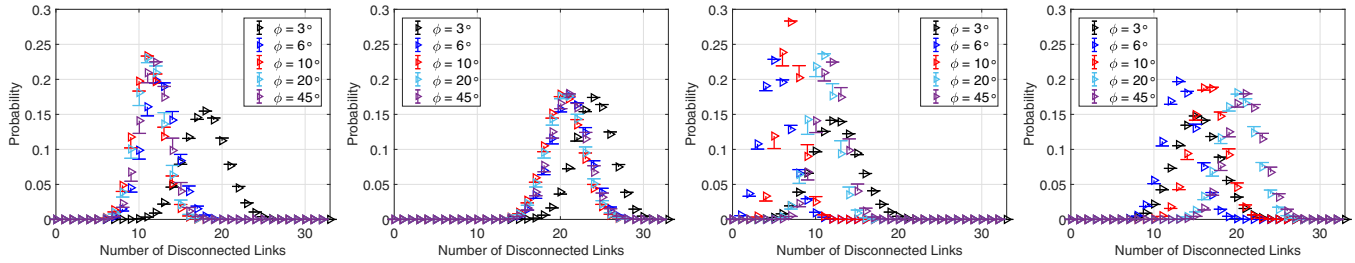

(a) $\lambda = 0.065$, $\sigma = 1$, $T = 3\,\mathrm{dB}$ (b) $\lambda = 0.065$, $\sigma = 1$, $T = 10\,\mathrm{dB}$ (c) $\lambda = 0.065$, $\sigma = 5$, $T = 3\,\mathrm{dB}$ (d) $\lambda = 0.065$, $\sigma = 5$, $T = 10\,\mathrm{dB}$

Fig. 6. High vehicle density/Platooning case with triangle markers and horizontal lines displaying the analytical and simulation results, respectively. Average inter-vehicle distance is approximately $15\,\mathrm{m}$ with $D = 500\,\mathrm{m}$.

variance is implemented for $3°$ and $6°$.

Fig. 4 illustrates the connectivity performance for 6 links in a scenario in which the average distance between consecutive vehicles is $200\,\mathrm{m}$, which results in a wide alignment zone that covers most of the lateral displacement of the receiver vehicle. It can be noticed that the probability is almost 0 to have 0, 4, 5 or 6 disconnected links, whereas there is a finite probability to have 1, 2 or 3 disconnected links. When the SINR threshold is increased to be $10\,\mathrm{dB}$, the probability values change and shift towards a higher number of disconnected links, which is represented in Fig. 4b. It can be observed that such a shift occurs for all cases in which the SINR threshold is increased.

Figs. 4a and 4b illustrate that the connectivity performance has a low sensitivity to beamwidth regardless of the SINR threshold. However, in Figs. 4c and 4d, the implementation of higher σ results in less interference, thus narrowing the beams clearly maximizes the connectivity. Interestingly, in Fig. 4c the $3°$ beamwidth almost provides an entirely end-to-end connected network as the probability for zero disconnected links is almost 1. Furthermore, the difference in connectivity performance for different beamwidths becomes more distinct for higher SINR thresholds, as is shown in Fig. 4d. Also note that the deteriorated connectivity performance in Figs. 4b and 4d in comparison to Figs. 4a and 4c is mostly caused by the shorter critical transmission range due to the higher SINR threshold; the beam misalignment probability is of minor importance.

In general, increasing the number of vehicles on the road increases the total interference for each vehicle, and subsequently causes a decrease in critical transmission range and an increased number of disconnected links. Fig. 5 shows the connectivity performance for medium vehicle density and, in general, presents similar results as those in Fig. 4. However, note that due to an increased number of vehicles the plots in Fig. 5 have maximum disconnectivity probabilities for a higher number of disconnected links in comparison to Fig. 4. In other words, introducing more hops into the network increases the number of disconnected links and decreases their absolute probabilities. Note that the narrowest beamwidth provides the best connectivity in low/medium vehicle density scenarios regardless of σ and T.

In Fig. 5c and 5d it can be noticed that decreasing the beamwidth increases both the signal power and the interference component in SINR. Interestingly, in low and medium

vehicle density cases, the results imply that most of the disconnected links are caused by failure to reach the critical transmission range rather than by misalignment. For instance, in the set-up of Fig. 5c, the critical transmission range for beamwidths of 3°, 6°, 10°, 20° and 45° are approximately $430\,\mathrm{m}$, $230\,\mathrm{m}$, $150\,\mathrm{m}$, $110\,\mathrm{m}$ and $99\,\mathrm{m}$, respectively. Thus, under the conditions of this scenario, only the critical transmission range of a 3° or 6° wide beam is substantially greater than the average inter-vehicle distance, $\lambda^{-1} = 100\,\mathrm{m}$.

Fig. 6 presents the results of the high vehicle density case, which could be an implementation of platooning, and provides different inferences compared to Figs. 4 and 5. For instance, in Fig. 6a a 3° provides the worst connectivity, whereas a 20° beamwidth provides the best connectivity, with marginal differences to 10° and 45°, which illustrates the scope for beamwidth optimization. This phenomenon is caused by the closest consecutive vehicle being too close to enable transmitter beam expansion, hence not all in-lane lateral displacements of the receiver vehicles can be compensated for. Similarly, in Fig. 6b the 6°, 10°, 20° and 45° beamwidth scenarios display an almost identical connectivity performance, in contrast to the worst performance of the 3° beamwidth.

The 6° beamwidth is the best performer in Fig. 6c. In this scenario, the critical transmission ranges for 3°, 6°, 10°, 20° and 45° are approximately $66\,\mathrm{m}$, $36\,\mathrm{m}$, $24\,\mathrm{m}$, $17\,\mathrm{m}$ and $16\,\mathrm{m}$, respectively, and the average consecutive vehicle distance is $15\,\mathrm{m}$. Nevertheless, the misalignment probabilities are 0.37, 0.075, 0.0043, 0.0018 and 0.0018, respectively. This phenomenon implies that with increasing beamwidth the cause of the disconnected links changes from misalignment to failure in reaching the critical transmission range. Hence, even though 3° provides a substantially greater critical transmission range, its tendency to misalignment hence makes a 6° beamwidth a better choice. Also, note that in some cases there is a trade-off between the number of disconnected links and their probabilities. For instance, in Fig. 6d the 6° beamwidth provides less disconnected links with a higher probability, whereas the 3° beamwidth provides more disconnected links with a lower probability.

V. Conclusions

In this work, the analytical connectivity analysis of mmWave V2V networks was based on a parametric critical transmission range and a beam misalignment probability caused by the lateral displacement of vehicles, and was validated by Monte Carlo simulations. In addition to stochastic geometry, geometric probability tools were used, that had been developed to calculate the probability of covering all gaps of a circle by uniformly and independently distributed arcs. In order to maximize connectivity, we have shown that there are different beamwidth regimes depending upon road curvature and vehicle density. In general terms, on low-curvature roads and for low/medium vehicle densities, the connectivity performance is nearly independent of the beamwidth. Moreover, for high vehicle density and low-curvature roads, wide beamwidths outperform narrow beamwidths. For other scenarios the best performance is obtained with narrowest beams. And finally, we have also characterized the trade-off between critical transmission range and misalignment probability.

References

[1] S. Kim *et al.*, "Multivehicle cooperative driving using cooperative perception: Design and experimental validation," *IEEE Trans. Intell. Transp. Syst.*, vol. 16, no. 2, pp. 663–680, Apr. 2015.

[2] R. Woodman *et al.*, "A human factors approach to defining requirements for low-speed autonomous vehicles to enable intelligent platooning," in *2019 IEEE Intel. Vehicles Symp. (IV)*, Paris, June 2019.

[3] S. Kwon, Y. Kim, and N. B. Shroff, "Analysis of connectivity and capacity in 1-D vehicle-to-vehicle networks," *IEEE Trans. Wireless Commun.*, vol. 15, no. 12, pp. 8182–8194, Dec. 2016.

[4] J. B. Kenney, "Dedicated short-range communications (DSRC) standards in the United States," *Proc. IEEE*, vol. 99, no. 7, pp. 1162–1182, July 2011.

[5] E. Kampert, P. A. Jennings, and M. D. Higgins, "Investigating the V2V millimeter-wave channel near a vehicular headlight in an engine bay," *IEEE Commun. Lett.*, vol. 22, no. 7, pp. 1506–1509, July 2018.

[6] O. Alluhaibi *et al.*, "Impact of Overlapped AoAs on the Achievable Uplink Rate of Hybrid Beamforming for Massive MIMO mm-Wave Systems for Industrial Environments," *IEEE Access*, vol. 7, pp. 101 178–101 194, July 2019.

[7] N. Wisitpongphan *et al.*, "Routing in sparse vehicular ad hoc wireless networks," *IEEE J. Sel. Areas Commun.*, vol. 25, no. 8, pp. 1538–1556, Oct. 2007.

[8] P. Santi and D. M. Blough, "The critical transmitting range for connectivity in sparse wireless ad hoc networks," *IEEE Trans. Mobile Comput.*, vol. 2, no. 1, pp. 25–39, Jan. 2003.

[9] M. Khabazian and M. K. M. Ali, "A performance modeling of connectivity in vehicular ad hoc networks," *IEEE Trans. Veh. Technol.*, vol. 57, no. 4, pp. 2440–2450, July 2008.

[10] X. Lin and J. G. Andrews, "Connectivity of millimeter wave networks with multi-hop relaying," *IEEE Wireless Commun. Lett.*, vol. 4, no. 2, pp. 209–212, Apr. 2015.

[11] K. Eshteiwi *et al.*, "Performance analysis of full-duplex vehicle relay-based selection in dense multi-lane highways," *IEEE Access*, 2019.

[12] S. Sun *et al.*, "Investigation of prediction accuracy, sensitivity, and parameter stability of large-scale propagation path loss models for 5G wireless communications," *IEEE Trans. Veh. Technol.*, vol. 65, no. 5, pp. 2843–2860, May 2016.

[13] Z. Pi and F. Khan, "An introduction to millimeter-wave mobile broadband systems," *IEEE Commun. Mag.*, vol. 49, no. 6, pp. 101–107, June 2011.

[14] L. Breiman, "The poisson tendency in traffic distribution," *Ann. Math. Statist.*, vol. 34, no. 1, pp. 308–311, Mar. 1963.

[15] S. M. Ross, *Stochastic processes*, 2nd ed. Hoboken, NJ, USA: Wiley, 1996.

[16] J. Wildman *et al.*, "On the joint impact of beamwidth and orientation error on throughput in directional wireless poisson networks," *IEEE Trans. Wireless Commun.*, vol. 13, no. 12, pp. 7072–7085, Dec. 2014.

[17] M. Ozpolat *et al.*, "A grid-based coverage analysis of urban mmwave vehicular ad hoc networks," *IEEE Commun. Lett.*, vol. 22, no. 8, pp. 1692–1695, Aug. 2018.

[18] A. W. Ahmed *et al.*, "Pavement performance follow-up and evaluation of polymer-modified test sections," *Int. J. Pavement Eng.*, pp. 1–14, 2018.

[19] "Lateral distribution of motorway traffic," Transport Research Laboratory, Wokingham, UK, Tech. Rep., 1998. [Online]. Available: https://trl.co.uk/sites/default/files/TRL356.pdf

[20] W. L. Stevens, "Solution to a geometrical problem in probability," *Ann. of Human Genetics*, vol. 9, no. 4, pp. 315–320, 1939.

[21] H. Solomon, *Geometric Probability*, Philadelphia, PA, USA: SIAM, 1978.